J. Fluid Mech. (2011), *vol.* 667, *pp.* 463–473.
doi:10.1017/S0022112010005628

Infrared Reynolds number dependency of the two-dimensional inverse energy cascade

ANDREAS VALLGREN†

Linné FLOW Centre, KTH Mechanics, SE-100 44 Stockholm, Sweden

(Received 3 May 2010; revised 21 October 2010; accepted 21 October 2010)

High-resolution simulations of forced two-dimensional turbulence reveal that the inverse cascade range is sensitive to an infrared Reynolds number, $Re_\alpha = k_f/k_\alpha$, where k_f is the forcing wavenumber and k_α is a frictional wavenumber based on linear friction. In the limit of high Re_α, the classic $k^{-5/3}$ scaling is lost and we obtain steeper energy spectra. The sensitivity is traced to the formation of vortices in the inverse energy cascade range. Thus, it is hypothesized that the dual limit $Re_\alpha \to \infty$ and $Re_v = k_d/k_f \to \infty$, where k_d is the small-scale dissipation wavenumber, will lead to a steeper energy spectrum than $k^{-5/3}$ in the inverse energy cascade range. It is also found that the inverse energy cascade is maintained by non-local triad interactions.

Key words: homogeneous turbulence, turbulence simulation, turbulence theory

1. Introduction

Kraichnan (1967) and Leith (1968) predicted the presence of two inertial ranges in two-dimensional turbulence, as a consequence of the twin invariants energy and enstrophy in the inviscid limit. The predicted spectra of the inertial ranges follow from scaling arguments, which give an energy spectrum $\propto k^{-5/3}$ in the energy inertial range at large scales, and a k^{-3} energy spectrum in the forward enstrophy cascade at smaller scales. Both of these predictions have been supported to various degrees by direct numerical simulations over the years. For the enstrophy cascade, the Navier–Stokes equation provides a sink of enstrophy by molecular viscosity at the smallest scales, and thus there is no need to provide any artificial removal mechanism. However, in order to extend the enstrophy inertial range, hyperviscosity is often introduced to replace the Navier–Stokes viscosity, with no significant effects on the energy spectrum (e.g. McWilliams 1984). For the inverse energy cascade, on the other hand, there is no natural sink of energy, and, to prevent an energy condensate to form at the largest scales, a large-scale friction is often introduced to mimic the large-scale drag present to some degree in both experiments and in quasi-two-dimensional flows, when rigid boundaries are present (e.g. Paret & Tabeling 1998 and Bruneau & Kellay 2005). Smith & Yakhot (1994) showed that if both the inverse energy cascade and the direct enstrophy cascade are well resolved, the energy spectrum in the energy inertial range steepens from $k^{-5/3}$ to $\sim k^{-2}$. This has been confirmed by high-resolution numerical simulations by Scott (2007), who also provided quantitative estimates when this transition occurs, by comparing the forcing wavenumber k_f with the largest resolved wavenumber k_m. He found that when $k_m/k_f \geqslant 16$, the $k^{-5/3}$ range steepens to k^{-2}. On

† Email address for correspondence: vallgren@mech.kth.se

the other hand, Boffetta (2007) showed that there is a very small cross-correlation between the energy and enstrophy fluxes in physical space which indicated that it is possible to generate a single cascade in numerical simulations (also supported by Tran & Bowman 2004). With even higher numerical resolution, Boffetta obtained a clean $k^{-5/3}$ range when $k_m/k_f \approx 55$. Also the experiments by Bruneau & Kellay (2005) gave support for the classic double cascade scenario. These differing results are a bit disturbing in the sense that whereas it would seem possible to generate a single energy cascade, the observed steepening in the presence of a well-resolved enstrophy cascade range clearly leads to a contradiction. Smith & Yakhot (1994) explained the steepening of the spectrum in terms of 'ultraviolet' vortices, formed at scales $k \gtrsim k_f$. Coherent vortices are hence a possible candidate. However, the development of a k^{-3} spectrum in the enstrophy inertial range would indicate the absence of strong vortices and influence from the large-scale drag (see Nam *et al.* 2000). Thus, it seems arguable that the large-scale drag might play an important role in the shape of the spectrum in the inverse cascade range, as also indicated by Sukoriansky, Galperin & Chekhlov (1999). This has been supported by several studies such as Borue (1994), who found strong vortices distributed over all scales in presence of a hypofrictional drag and later by Danilov & Gurarie (2001*a*, *b*). However, the application of a hypofrictional drag has been shown to be problematic as it introduces bottleneck effects, as demonstrated by Bos & Bertoglio (2009). It is the aim of this paper to investigate the role of particularly the large-scale linear friction, but, to a lesser degree, the small-scale viscosity as well, in the resulting shape of the energy spectrum in the inverse cascade range. This will be accomplished by the highest resolution simulations of the inverse energy cascade range reported so far.

2. Numerical method

The numerical experiments are based on simulations of the two-dimensional Navier–Stokes equation in a 2π-periodic domain with the addition of a random forcing f and a large-scale drag. Thus,

$$\frac{\partial \omega}{\partial t} + (\boldsymbol{u} \cdot \nabla)\omega = (-1)^{n+1}\nu\nabla^{2n}\omega + f - \alpha\omega, \tag{2.1}$$

where ν represents Navier–Stokes viscosity ($n = 1$) or hyperviscosity ($n > 1$) and α is the linear drag coefficient. The α-parameter has been determined from the relation

$$\alpha \sim \left(\frac{2\pi}{k_\alpha}\right)^{-2/3} \left(\frac{\eta}{k_f^2}\right)^{1/3}, \tag{2.2}$$

where k_α represents a hypothetical wavenumber where frictional effects become significant, k_f is the forcing wavenumber and η is the enstrophy injection rate, which is set to 1 in our simulations. The corresponding energy injection rate is thus η/k_f^2. The numerical integration forward in time is performed with a fourth-order Runge–Kutta method, with the time step restricted by a Courant–Friedrichs–Lewy (CFL) condition and dealiasing following an 8/9 method.

We perform a set of simulations with different resolutions ($N = 8192$ and $N = 16\,384$), with Navier–Stokes viscosity and hyperviscosity and various frictional coefficients. They are presented in table 1, where k_f refers to the peak forcing wavenumber in a narrow wavenumber shell. The ratio k_m/k_f is the highest resolved wavenumber over the forcing wavenumber, k_d/k_f is the ratio between the dissipation

https://doi.org/10.1017/S0022112010005628 Published online by Cambridge University Press

Run	Res.	k_f	k_m/k_f	k_d/k_f	k_f/k_α	n	ν	α	t_{max}	β	γ	$\mathscr{C}$	$\epsilon_\omega^\alpha/\eta$	ϵ_ω/η	$\epsilon_L k_f^2/\eta$	F_ω
A	8192	200	25	6.4	289	1	6×10^{-7}	6×10^{-3}	15.3	−1.7	−4.2	5.0	0.07	0.93	0.85	4.3
B	8192	200	25	6.4	307	4	10^{-25}	6×10^{-3}	9.3	−2.0	−3.7	–	0.10	0.90	0.96	7.6
C	8192	300	17	4.3	757	1	6×10^{-7}	3×10^{-3}	11.9	−1.7	−4.5	4.1	0.03	0.97	0.78	3.8
D	8192	1000	5	1.3	1044	4	10^{-25}	2×10^{-3}	23.2	−1.7	−7.0	5.6	0.01	0.99	0.46	4.8
E	16 384	1000	10	2.4	2600	4	9×10^{-28}	10^{-3}	6.1	−2.4	−4.5	–	0.02	0.98	0.84	22.4
F	16 384	1000	10	2.4	324	4	9×10^{-28}	6×10^{-3}	7.1	–	−4.5	–	0.07	0.93	0.83	10.4
G	16 384	2000	5	1.3	3857	4	5×10^{-28}	9×10^{-4}	11.4	−2.0	−7.0	–	0.005	0.99	0.46	8.8

TABLE 1. Simulation parameters and statistics.

wavenumber, $k_d = \nu^{-1/2n}\eta^{1/6n}$, and the forcing wavenumber, and k_f/k_α denotes the ratio between the forcing wavenumber and a frictional wavenumber, which we estimate as $k_\alpha = 2\pi C_\alpha(\alpha^3/\epsilon_L)^{1/2}$, where ϵ_L is the energy dissipation rate at large scales and C_α is a constant which is not known *a priori* and is set to unity here. This might give rise to $k_\alpha < 1$ but enables direct comparison with other studies. The true frictional scale can be determined *a posteriori* and, in general, $C_\alpha > 1$ (see e.g. Danilov & Gurarie 2001*a*). The parameter t_{max} refers to the length of the simulation in non-dimensional time units, normalized by $E/\epsilon = Ek_f^2/\eta$, where E is the total energy and ϵ is the energy dissipation rate. Runs B, D, E, F and G were run with hyperviscosity ($n = 4$), otherwise with Navier–Stokes viscosity. In table 1, a set of statistics is also presented. The parameter β denotes the estimated slope k^β of the energy spectrum in the energy inertial range and γ is the corresponding exponent in the direct enstrophy cascade range. In case of a $k^{-5/3}$ spectrum, $\mathscr{C} = \langle E(k)\epsilon^{-2/3}k^{5/3}\rangle_{k_p<k<k_f}$, where k_p is the peak energy wavenumber. The parameter $\epsilon_\omega^\alpha/\eta$ corresponds to the fraction of the injected enstrophy rate that is dissipated by the large-scale drag, whereas ϵ_ω/η corresponds to that dissipated by the small-scale viscosity and $\epsilon_L k_f^2/\eta$ is the energy dissipation rate at large scales, normalized by the energy injection rate. The vorticity flatness F_ω is also given, which is the spatially and temporally (in the quasi-stationary state) averaged flatness of vorticity: $F_\omega = \langle\omega^4\rangle/\langle\omega^2\rangle^2$.

3. Results

Scott (2007) argued that the forcing Reynolds number, $Re_f \sim k_m^2/k_f^2$, should influence the steepness of the spectrum in the energy cascade range beyond a critical value, which he estimated to $\sqrt{Re_f} \sim 16$. To test this prediction, we perform a set of simulations forced at $k_m/k_f = [5, 17, 25]$ for $N = 8192$ and $k_m/k_f = [5, 10, 34]$ for $N = 16\,384$. We begin by presenting the results from the $N = 8192$ simulations A, C and D. Scott suggested that when $k_m/k_f \geqslant 16$, intermittency measures become significant and departures from a $k^{-5/3}$ range would manifest. In our simulations, the $k^{-5/3}$ ranges are rather clean (see figure 1*a*). Differences are mainly manifested in the constant $\mathscr{C}$ (see table 1) which is around 5.0 in run A, 4.1 in run C and 5.6 in run D, which is a little bit lower than observed by Boffetta (2007). Vorticity flatness values are low as $F_\omega \leqslant 5$, which is in agreement with, e.g., Maltrud & Vallis (1991) and Paret & Tabeling (1998), signifying the absence of vortices. All three simulations have an energy flux that varies slightly through the energy cascade range (see figure 1*b*), as expected in the presence of a linear drag (see Danilov & Gurarie 2001*b*). We also see that the fraction of energy injected and transferred to large scales differ between the runs (table 1 and figure 1*b*), with approximately 85 % transferred to larger scales in run A, 78 % in run C and 46 % in run D. Thus, only a fraction of the total energy injection is transferred to large scales in run D, but we still obtain a $k^{-5/3}$ range, as also found by Tran & Bowman (2004). However, as can be seen in figure 1(*c*), none of the simulations, A, B or C, show a constant enstrophy flux in the direct enstrophy cascade range, and the spectral slopes are quite steep (see table 1). Thus, we perform a simulation (B) similar to A, but with the use of hyperviscosity. A comparison between runs A and B (figure 1*a*) reveals that the energy spectrum is steeper in B and that there is an extensive range of constant enstrophy flux (figure 1*c*). We obtain an energy spectrum $E(k) \sim k^{-2}\ \forall\ k/k_f \in (0.3, 0.9)$. This is in qualitative agreement with the results by Smith & Yakhot (1994) and Scott (2007). The deviation from the $k^{-5/3}$ spectrum develop as a result of stronger vortices, reflected by an increase in F_ω from 4.3 in run A to 7.6 in run B. We also performed a simulation similar to C but with a

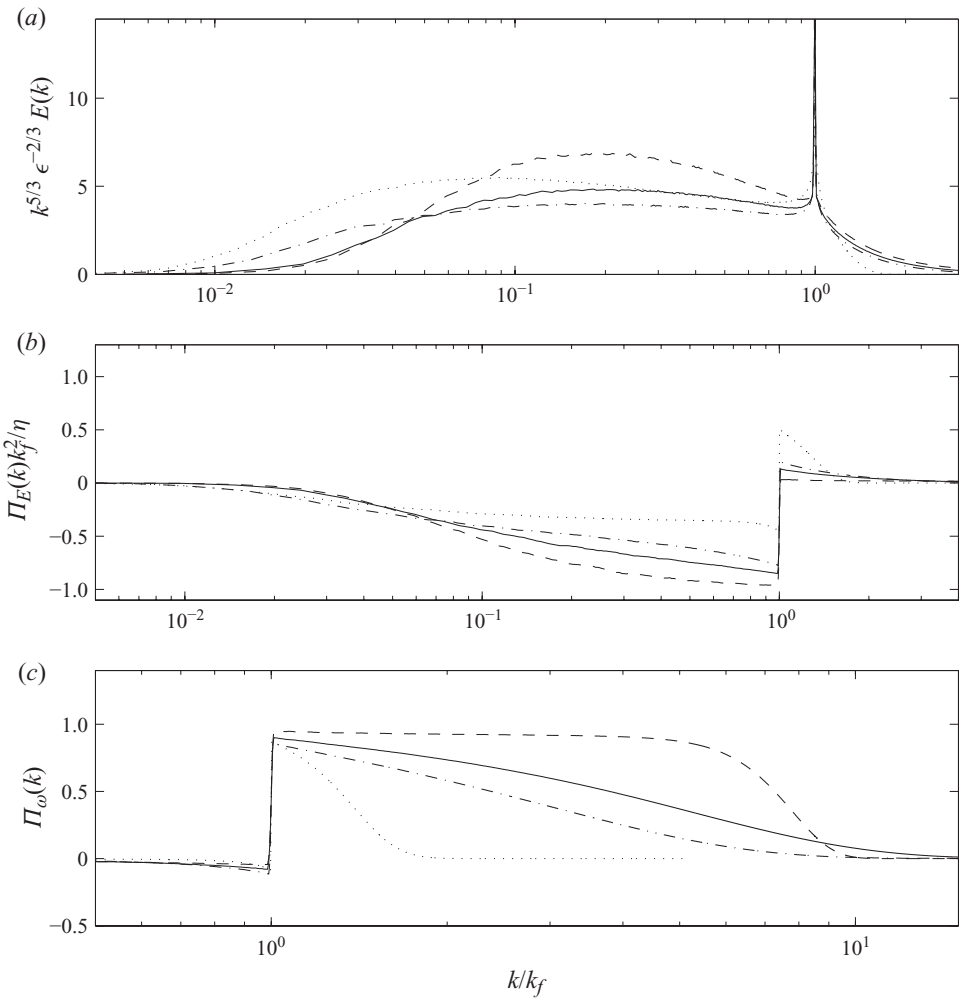

FIGURE 1. (*a*) Compensated energy spectra from runs A (solid line), B (dashed line), C (dashed–dotted line) and D (dotted line). (*b*) Energy flux normalized by energy injection rate. (*c*) Enstrophy flux.

resolution $N = 16\,384$ and with hyperviscosity, which resulted in a steepening of the energy spectrum to $\sim k^{-2}$.

To test whether the results show any dependence on the infrared Reynolds number $Re_\alpha = k_f/k_\alpha$ and scale separation k_d/k_α, we perform higher resolution simulations. Runs E and F are run with hyperviscosity but with different strength of the linear drag. Beginning with run E, we obtain an energy spectrum which is substantially steeper than $k^{-5/3}$, with a spectral slope $\beta \approx -2.4$ over a substantial range of scales. In figure 2(*a*), the compensated energy spectra ($k^{5/3}\epsilon^{-2/3}E(k)$) are shown. The energy flux is nearly constant in this range, with approximately 84 % of the injected energy transferred to larger scales (figure 2*b*). There is also a short constant enstrophy flux range in the forward enstrophy cascade range and the slope of the energy spectrum in this range is about −4.5. To test whether a single (energy) cascade range would yield a different result, we perform simulation G. The constant enstrophy flux range is now eliminated (figure 2*c*) and the energy spectrum steepens to $\gamma \sim -7$ at high

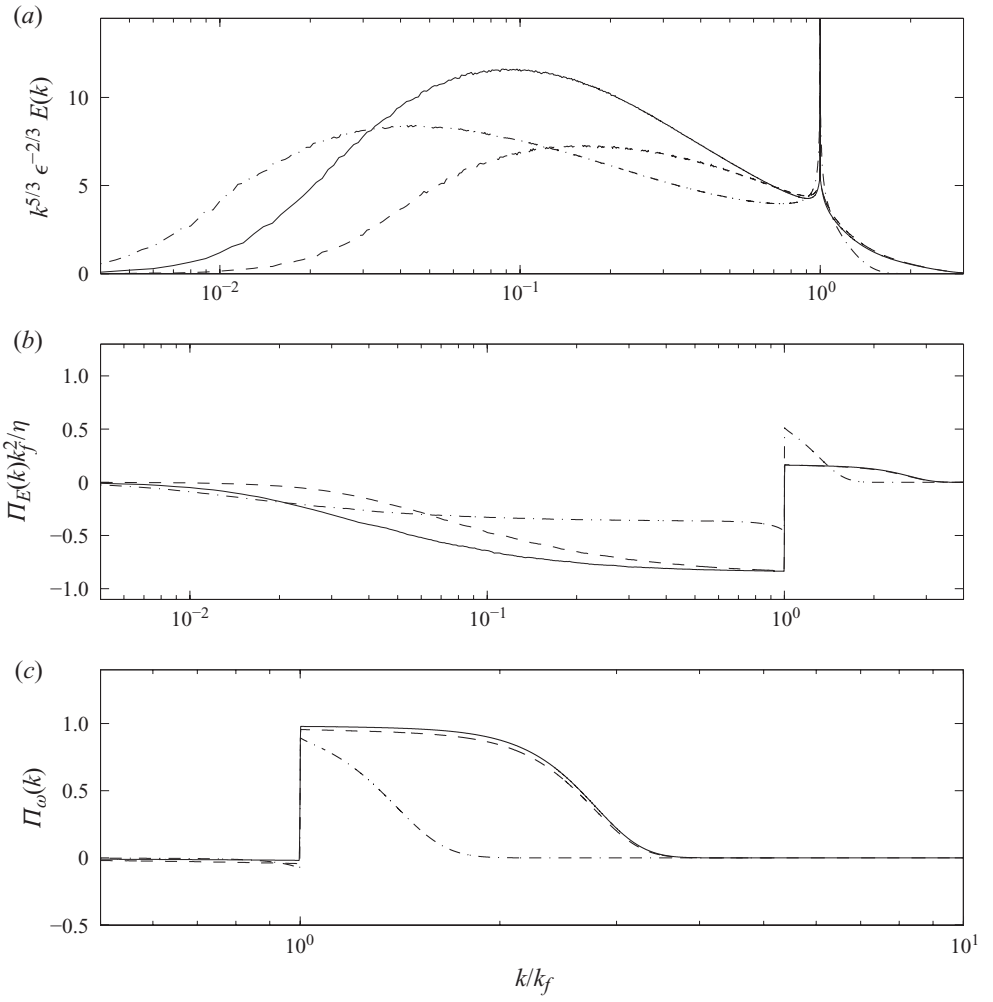

FIGURE 2. (*a*) Compensated energy spectra ($k^{5/3}$) from runs E (solid line), F (dashed line) and G (dashed–dotted line). (*b*) Energy flux normalized by energy injection rate. (*c*) Enstrophy flux.

wavenumber. As for run D, about 46 % of the injected energy is transferred to larger scales (figure 2*b*) and there is a constant flux range. However, the energy spectrum is steeper than $k^{-5/3}$ with a clean k^{-2} spectrum over more than a decade. Thus, the effect of reducing Re_v is not enough to retain the Kolmogorov spectrum. By increasing the linear drag coefficient six times in run F compared to run E, we see in figure 2(*a*) that the energy spectrum shallows in the inverse cascade range. The energy flux is no longer constant in F as the increased Ekman drag affects a broader range of scales, whereas the enstrophy flux is practically undisturbed (figure 2*c*). The stronger friction in F acts to reduce the strength of the vortices, as the vorticity flatness is reduced by more than a factor of 2 (see table 1).

To gain insight into the physical differences between the simulations, snapshots of the real vorticity fields from runs A and E are presented in figure 3(*a*). Run A corresponded to a simulation with a $k^{-5/3}$ spectrum and a relatively low-vorticity flatness. The vorticity field (*a*, left) has been zoomed in by a factor of 64, revealing

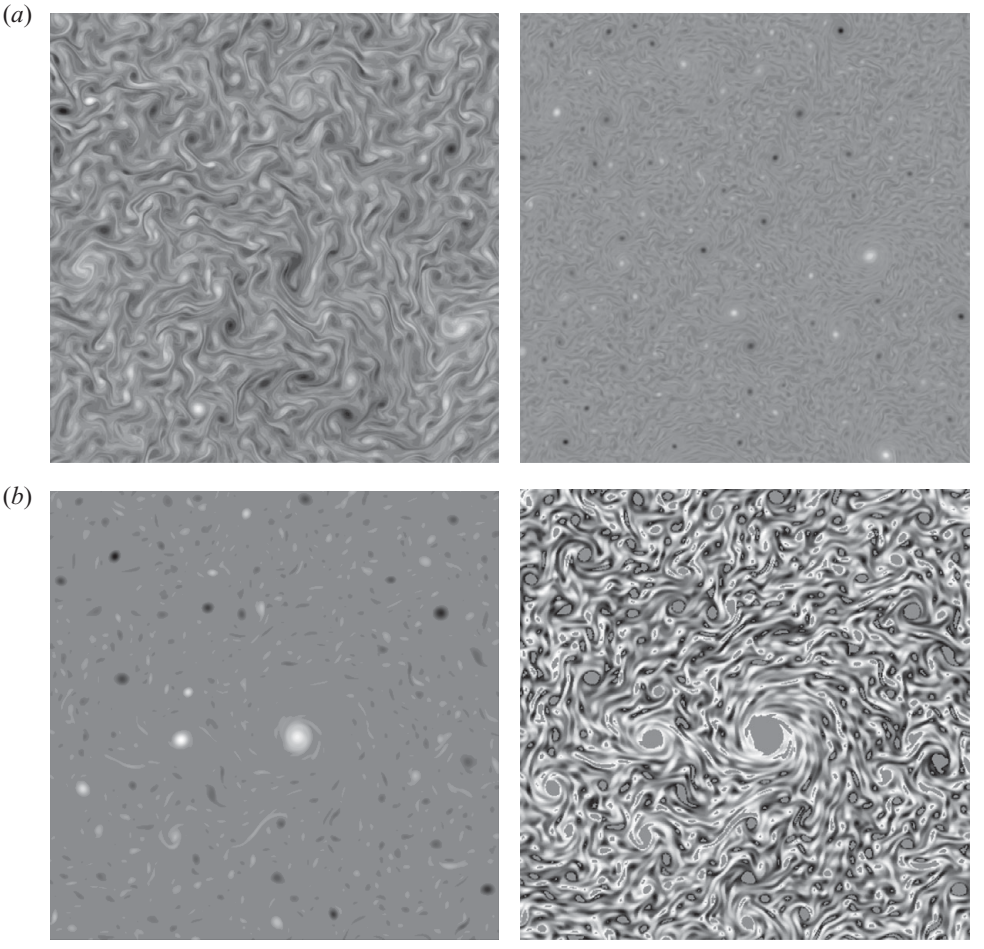

FIGURE 3. (*a*) Snapshots of vorticity from run A (left, zoomed in to 1:64 of the domain), run E (right, zoomed in to 1:256 of the domain). (*b*) Filtered vorticity fields showing the vortex subfield (left) and background field (right) of run E, respectively.

that vortices are smeared out. Thus, although vortices exist, they are not dominating the picture. The highest vorticity flatness measure was found in run E and its vorticity field is shown in figure 3 (*a*, right), which has been zoomed in by a factor of 256. Isolated and relatively strong vortices are observed. To quantify the effect of these vortices regarding the energy spectra and energy fluxes, the vorticity field has been decomposed into a vortex and background subfield following Borue (1994). This is essentially achieved by setting $\omega = 0$ for $|\omega| < 2\omega_{r.m.s.}$ for the vortex subfield and vice versa for the background subfield. This procedure is implemented for runs B, E, F and G, all of which showed energy spectra steeper than $k^{-5/3}$ in the inverse cascade range. The effect of doing this in physical space is demonstrated in figure 3(*b*), where the left subfigure shows the vortex subfield whereas the right figure shows the background subfield. Note that these two figures correspond to a fraction of 1/1024 of the whole domain. It can first be noted that the vortex subfields generally contain beyond 50 % more energy and enstrophy than the background fields. The resulting energy spectra for the vortex and background vorticity fields are presented in figure 4(*a*) and (*b*), respectively. It becomes immediately clear that the vortex fields

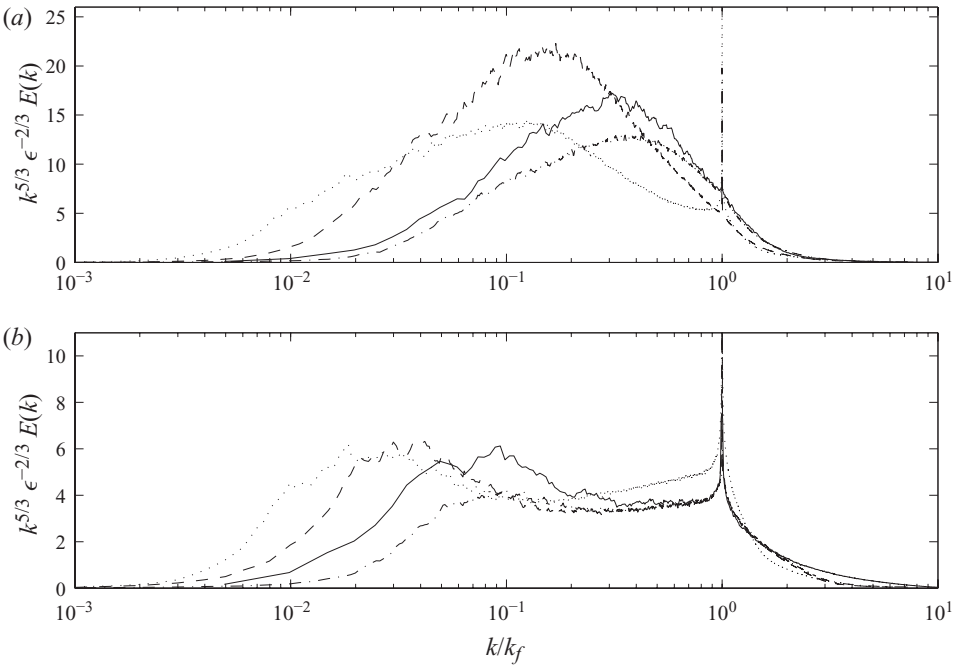

FIGURE 4. (*a*) Compensated energy spectra ($k^{5/3}$) for the vortex part of runs B (solid line), E (dashed line), F (dashed–dotted line) and G (dotted line). (*b*) Compensated energy spectra for the background field.

show substantially steeper spectra, $E(k) \propto k^{-2} \rightarrow k^{-3}$. The peak energy wavenumbers are different between the simulations and are shifted towards the forcing scale with increasing friction. The enstrophy spectra (not shown) reveal that the peak vorticity is found at scales up to more than six times larger than the forcing scale. Thus, the vortices constitute a substantial part of the inverse energy cascade range, particularly in runs E and G. The background fields, on the other hand, show spectra that are closer to $k^{-5/3}$ over a substantial range of scales. Both the energy and the enstrophy fluxes (not shown) signal qualitatively similar behaviour.

To explain the formation of vortices near the forcing scales, and the survival of these into a substantial part of the inverse cascade range, the dissipation spectra are investigated. It is found that 5–10 % of the vorticity is dissipated by the kinematic viscosity at small wavenumber, $k < k_f$, for runs A, C, D and G, whereas 3–5 % is dissipated in a narrow wavenumber shell enclosing the forcing range. As for the energy, about 50 % of the energy is dissipated at small wavenumber in runs A and C whereas 5–10 % is dissipated in the vicinity of the forcing scales. For runs D and G, approximately 15 % of the energy is dissipated at small wavenumber and 5–7 % at the forcing scales. In runs B, E and F, there is nearly no loss of either vorticity nor energy by the kinematic viscosity at small wavenumber, including the forcing scales. The linear drag, on the other hand, has a more even dissipation distribution, since it is less scale selective than the kinematic viscosity, but there is nearly no loss of energy by the drag at the forcing scales and larger wavenumber in runs E, F and G.

The steepening of the energy spectra in the inverse energy cascade range suggests that the inverse energy cascade may not be maintained by local interactions in Fourier

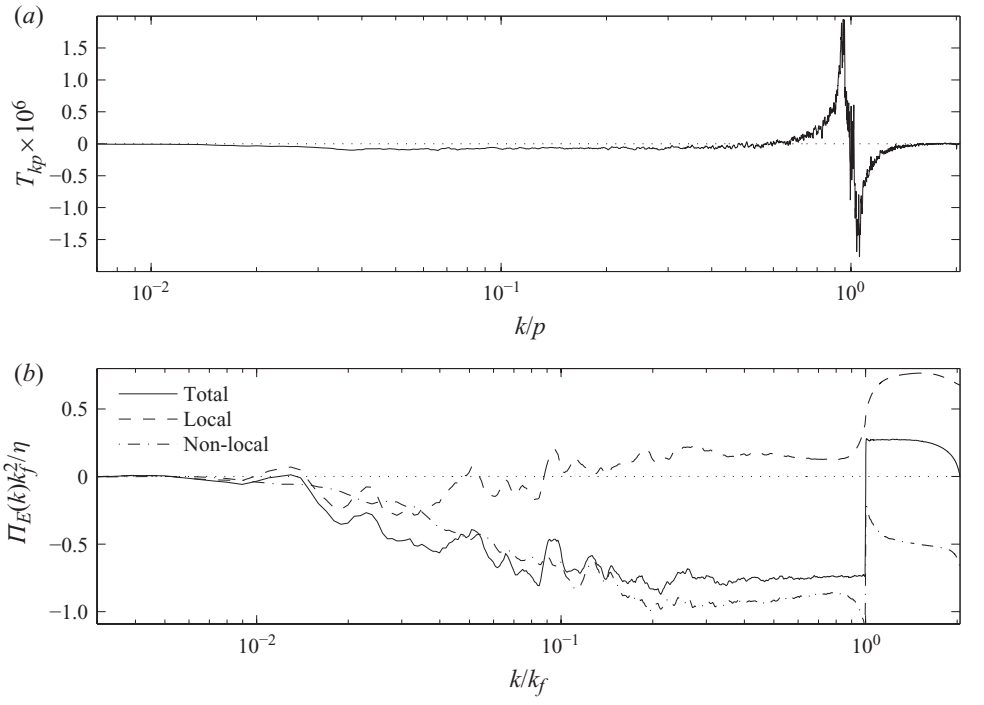

FIGURE 5. (*a*) Energy transfer from wavenumber $k=1000$ to wavenumber p for run G. (*b*) Energy flux for run E decomposed into local, non-local and total parts. The abscissa is wavenumber k normalized by p (*a*) and k_f (*b*), respectively.

space. To investigate this, the transfer function,

$$T_{\boldsymbol{kpq}} = k_j \mathrm{Im}[\widehat{u_j}(\boldsymbol{q})\widehat{u_i}(\boldsymbol{p})\widehat{u_i}^*(\boldsymbol{k})], \tag{3.1}$$

is studied. Here, $\boldsymbol{q}=\boldsymbol{k}-\boldsymbol{p}$, and the hat represents the Fourier transform. After integration over an azimuthal angle in $\boldsymbol{k}$-space, $T_{\boldsymbol{kpq}}$ can be written as a function, T_{kpq}, of the scalar wavenumbers k, p and q. In turn, T_{kpq} can be written as a function, T_{kp}, of k and p, after integration over q. This allows for analysis of wavenumber shell interactions (see, e.g., Maltrud and Vallis 1993, Danilov and Gurarie 2001*a* and Verma *et al.* 2005). It is found that the triad interactions are highly non-local but that the energy transfer is mostly local and *forward* between wavenumber shells, as can be inferred from figure 5 and as also found in a number of studies (Maltrud and Vallis 1993; Danilov and Gurarie 2001*a*; Verma *et al.* 2005). Figure 5(*a*) shows the energy transfer T_{kp} for run G at $k=1000$, which is in the middle of the energy inertial range. There is a small but consistent non-local transfer of energy from large wavenumber to much smaller wavenumber. This suggests that the basic mechanism for the inverse energy flux might be non-local in its character. By increasing α, the relative importance of the non-local interactions has been found to be reduced (not shown), as the large-scale friction damps the interactions involving large scales, that is, small p and q. This is reflected by a suppression of T_{kp} at low wavenumber. To quantify the local and non-local contribution to the energy flux $\Pi(k) = -\sum_0^k \sum_p \sum_q T_{kpq}$, a locality threshold was defined such that $(p \wedge q)/k \in [0.2, 5]$ corresponds to the local contribution and the non-local contribution comes from $(p \vee q)/k < 0.2$ and $(p \vee q)/k > 5$. Figure 5(*b*) shows the result from run E, which shows a result similar to

all the other simulations. The total energy flux in the energy inertial range is negative and is completely maintained by the non-local contribution. The small contribution from local interactions is in fact positive. Another finding is that there is a weak but persistent coupling between the large scales and much smaller scales located in the enstrophy cascade range, when this is present, manifested in an energy transfer from the small scales to the large scales.

4. Discussion and conclusions

It is meaningful to ask whether it is actually possible to obtain the classic double cascade scenario as theoretized by Kraichnan–Batchelor–Leith in the limit of two high Reynolds numbers, Re_α and Re_ν. On the basis of the numerical results, it can be hypothesized that the classic energy inertial range hypothesis with $k^{-5/3}$ is a combined low Re_α and low Re_ν effect. For low Re_α and high Re_ν, we essentially confirm the results by Scott (2007). When the enstrophy cascade is well resolved, we obtain relatively steeper energy spectra in the energy cascade range, compared to the simulations where the enstrophy cascades are absent or much reduced. The suggested mechanism is a weak non-local coupling between the energy inertial range and the enstrophy cascade range. In physical space, it might be connected to the observations by Elhmaidi, von Hardenberg & Provenzale (2005). However, for large Re_α, this mechanism is of less importance, as demonstrated by run G. In this run, $\gamma = -7$, indicating the absence of an enstrophy inertial range, but the energy spectrum in the energy range is still steeper than $-5/3$. This may be explained by a significant non-local transfer of energy, which bears the sole responsibility for the inverse energy flux, which is consistent with the results of Maltrud & Vallis (1993). These results indicate that the $k^{-5/3}$ spectra may not be universal. A comparison with Boffetta (2007) shows that $Re_\alpha \in \sim(200, 400)$ in his simulations, whereas $Re_\nu \in \sim(4, 18)$. Thus, Re_α is always low and the Navier–Stokes viscosity is effective over relatively broad scales.

To conclude, we have performed a number of simulations spanning a range of Re_α and Re_ν. Our results suggest that the inertial energy range spectrum is sensitive to both Re_α and Re_ν. In physical space, the sensitivity is traced to the formation of vortices in the inverse energy cascade range. These can be distorted by either placing the forcing in, or very near, the ultraviolet dissipation range, or by applying a strong enough infrared linear friction. In spectral space, the departure from the classic scaling of the energy spectrum is associated with a strong degree of non-locality *in conjunction* with either $Re_\alpha \to \infty$ or $Re_\nu \to \infty$. It is thus hypothesized that the simultaneous limit of $Re_\alpha \to \infty$ and $Re_\nu \to \infty$ will always lead to an energy spectrum steeper than $k^{-5/3}$ in the energy inertial range, at least if no specially designed dissipation operator, such as employed by Sukoriansky, Galperin & Chekhlov (1999), is utilized.

Computer time was provided by the Swedish National Infrastructure for Computing (SNIC) with a generous grant by the Knut and Alice Wallenberg Foundation. E. Lindborg and the anonymous reviewers are gratefully acknowledged for fruitful discussions.

REFERENCES

Boffetta, G. 2007 Energy and enstrophy fluxes in the double cascade of two-dimensional turbulence. *J. Fluid Mech.* **589**, 253.

Borue, V. 1994 Inverse energy cascade in stationary two-dimensional homogeneous turbulence. *Phys. Rev. Lett.* **72**, 1475.

Bos, W. J. T. & Bertoglio, J.-P. 2009 Large-scale bottleneck effects in two-dimensional turbulence. *J. Turbul.* **10**, 1.

Bruneau, C. H. & Kellay, H. 2005 Experiments and direct numerical simulations of two-dimensional turbulence. *Phys. Rev.* E **71**, 046305-1.

Danilov, S. & Gurarie, D. 2001*a* Forced two-dimensional turbulence in spectral and physical space. *Phys. Rev.* E **63**, 061208.

Danilov, S. & Gurarie, D. 2001*b* Nonuniversal features of forced two-dimensional turbulence in the energy range. *Phys. Rev.* E **63**, 020203-1.

Elhmaidi, D., von Hardenberg, J. & Provenzale, A. 2005 Large scale dissipation and filament instability in two-dimensional turbulence. *Phys. Rev. Lett.* **95**, 014503-1.

Kraichnan, R. H. 1967 Inertial ranges in two-dimensional turbulence. *Phys. Fluids* **10**, 1417.

Leith, C. E. 1968 Diffusion approximation for two-dimensional turbulence. *Phys. Fluids* **11**, 671.

Maltrud, M. E. & Vallis, G. K. 1991 Energy spectra and coherent structures in forced two-dimensional and beta-plane turbulence. *J. Fluid Mech.* **228**, 321.

Maltrud, M. E. & Vallis, G. K. 1993 Energy and enstrophy transfer in numerical simulations of two-dimensional turbulence. *Phys. Fluids* A **5**, 1760.

McWilliams, J. C. 1984 The emergence of isolated coherent vortices in turbulent flow. *J. Fluid Mech.* **146**, 21.

Nam, K., Ott, E., Antonsen, T. M. & Guzdar, P. N. 2000 Lagrangian chaos and the effect of drag on the enstrophy cascade in two-dimensional turbulence. *Phys. Rev. Lett.* **84**, 5134.

Paret, J. & Tabeling, P. 1998 Intermittency in the two-dimensional inverse cascade of energy: experimental observations. *Phys. Fluids* **10**, 3126.

Scott, R. K. 2007 Nonrobustness of the two-dimensional turbulent inverse cascade. *Phys. Rev.* E **75**, 046301.

Smith, L. M. & Yakhot, V. 1994 Finite-size effects in forced two-dimensional turbulence. *J. Fluid Mech.* **274**, 115.

Sukoriansky, S., Galperin, B. & Chekhlov, A. 1999 Large scale drag representation in simulations of two-dimensional turbulence. *Phys. Fluids* **11**, 3043.

Tran, C. V. & Bowman, J. C. 2004 Robustness of the inverse energy cascade in two-dimensional turbulence. *Phys. Rev.* E **69**, 036303.

Verma, M. K., Ayyer, A., Debliquy, O., Kumar, S. & Chandra, A. V. 2005 Local shell-to-shell energy transfer via nonlocal interactions in fluid turbulence. *Pramana* **65**, 297.